AGU PUBLICATIONS

JGR

Journal of Geophysical Research: Space Physics

RESEARCH ARTICLE
10.1002/2016JA022916

Electron flux dropouts at Geostationary Earth Orbit: Occurrences, magnitudes, and main driving factors

R. J. Boynton[1], D. Mourenas[2], and M. A. Balikhin[1]

[1]Department of Automatic Control and Systems Engineering, University of Sheffield, Sheffield, UK, [2]CEA, DAM, DIF, Arpajon, France

Key Points:
- The magnitude of the dropouts remains nearly constant as electron energy increases up to 1 MeV, increasing strongly above 1 MeV
- There are much less numerous dropouts in the medium-energy range, between 63 keV and 450–650 keV than at E < 63 keV or E > 450–650 keV
- The factors governing the dropouts are the AE index at low energies and dynamic pressure coupled with southward IMF for high energies

Correspondence to:
R. J. Boynton,
rboynton85@gmail.com

Citation:
Boynton, R. J., D. Mourenas, and M. A. Balikhin (2016), Electron flux dropouts at Geostationary Earth Orbit: Occurrences, magnitudes, and main driving factors, *J. Geophys. Res. Space Physics*, *121*, 8448–8461, doi:10.1002/2016JA022916.

Received 6 MAY 2016
Accepted 17 AUG 2016
Accepted article online 22 AUG 2016
Published online 10 SEP 2016

Abstract Large decreases of daily average electron flux, or dropouts, were investigated for a range of energies from 24.1 keV to 2.7 MeV, on the basis of a large database of 20 years of measurements from Los Alamos National Laboratory (LANL) geosynchronous satellites. Dropouts were defined as flux decreases by at least a factor 4 in 1 day, or a factor 9 in 2 days during which a decrease by at least a factor of 2.5 must occur each day. Such decreases were automatically identified. As a first result, a comprehensive statistics of the mean waiting time between dropouts and of their mean magnitude has been provided as a function of electron energy. Moreover, the Error Reduction Ratio analysis was applied to explore the possible nonlinear relationships between electron dropouts and various exogenous factors, such as solar wind and geomagnetic indices. Different dropout occurrences and magnitudes were found in three distinct energy ranges, lower than 100 keV, 100–600 keV, and larger than 600 keV, corresponding to different groups of drivers and loss processes. Potential explanations have been outlined on the basis of the statistical results.

1. Introduction

The near-dipolar configuration of the geomagnetic field allows charged energetic particles to remain trapped in a region known as the Van Allen radiation belts. As such, the radiation belts are composed of energetic electron from tens of keV to several MeV. These electrons can potentially pose a threat to astronauts health [*Maalouf et al.*, 2011] and cause havoc on spacecraft electronic systems [*Baker*, 2002; *Horne et al.*, 2013]. The population of energetic electrons can fluctuate by large amounts over very short time scales. Some of the most extreme fluctuations are called "dropouts" [*Green et al.*, 2004]. During a dropout, the population of trapped electrons can decrease by up to several orders of magnitude on a time scale of ~2–20 h. Although such phenomena can correspond in part to a mere radial redistribution of electron fluxes [*Kim and Chan*, 1997], many recent studies have shown that outer belt dropouts most often include true loss of electrons [e.g., see *Turner et al.*, 2012b, 2013, and references therein]. However, the mechanisms driving such fast and strong losses of outer radiation belt electron fluxes are still not yet fully understood, with many remaining questions [*Green et al.*, 2004; *Turner et al.*, 2013].

Losses of electrons in the outer radiation belt are thought to be caused by a number of different mechanisms: Magnetopause shadowing [*Kim and Chan*, 1997; *Bortnik et al.*, 2006; *Turner et al.*, 2012b] with enhanced outward radial diffusion [*Ukhorskiy et al.*, 2015], precipitation into the atmosphere [*Bailey*, 1968; *Bortnik et al.*, 2006], or adiabatic effects [*McIlwain*, 1966; *Kim and Chan*, 1997]. Magnetopause shadowing occurs when the magnetopause is abruptly compressed by the solar wind, allowing electrons drifting around the Earth on usually closed drift shells to escape in the open space. After the compressed magnetosphere expands back to its quiet time shape, there appears a large spatial gradient between the phase space density (PSD) of electrons close to Earth and PSD at farther locations where electrons have recently been lost. This spatial gradient of the PSD results in outward radial diffusion of electrons and a progressive loss of electrons initially present closer to the Earth: dropouts can extend this way down to lower *L* values.

Electron precipitation into the atmosphere is caused by resonant interactions between the trapped particles and plasma waves. This interaction can scatter electrons in pitch angle toward the loss cone, leading to their loss into the atmosphere. Electromagnetic ion cyclotron (EMIC) waves [*Summers and Thorne*, 2003], whistler mode chorus waves [*Lorentzen et al.*, 2001], and hiss waves [*Meredith et al.*, 2006], possibly aided by equatorial magnetosonic waves [*Balikhin et al.*, 2015; *Mourenas et al.*, 2013], have all been shown to efficiently scatter electrons in pitch angle.

Reversible adiabatic electron losses correspond simply to a redistribution in radial direction and are due to the conservation of the three adiabatic invariants [*Dessler and Karplus*, 1961]. Increases in the ring current during the main phase of a geomagnetic storm can decrease the strength of the geomagnetic field. This impels the electrons to decelerate to conserve the first adiabatic invariant and to move outward to conserve the third adiabatic invariant. This is often referred to as the "*Dst* effect," because geomagnetic storms increase the ring current, causing a reduction in the magnetic field in the inner magnetosphere. When the ring current recovers after the storm, the magnetic field will increase, thus reaccelerating the electrons and moving them inward [*Kim and Chan*, 1997].

The solar wind effects on electron flux dropouts were studied by *Borovsky and Denton* [2010] during geomagnetic storms, where they used a superposed epoch analysis. They found that the dropouts coincided with increases in solar wind dynamic pressure and southward IMF. A similar study was performed by *Yuan and Zong* [2013], where they analyzed the different effects of dynamic pressure and IMF orientation on the dropouts. They conclude that southward IMF and high pressure lead to the strongest dropouts, while the opposite of low pressure and a northward IMF leads to the weakest dropouts. Unlike these previous studies, which only focused on dropouts occurring during geomagnetic storms, *Gao et al.* [2015] recently investigated all dropouts occurring during storm or nonstorm periods, using 16 years of POES and GOES satellite data but focusing only on >2 MeV electrons. *Gao et al.* [2015] found that both the *z* component of the IMF and solar wind dynamic pressure have an influence on relativistic electron dropouts and that not all such events are caused by magnetopause shadowing. They suggested that southward IMF can often lead to increased >2 MeV electron precipitations, possibly due to interactions with intense duskside EMIC waves.

These past studies of the main solar wind parameters controlling electron dropouts have employed superposed epoch analysis. However, superposed epoch analysis is not able to accurately weigh the statistical influence of different variables effectiveness at the same time, or to identify any complex nonlinear relationship. The Nonlinear AutoRegressive Moving Average eXogenous input (NARMAX) Error Reduction Ratio (ERR) methodologies are able to determine and assess a wide class of complex nonlinear dependencies, such as identifying the solar wind parameters that control the magnitude of the dropout. This methodology has been applied to a wide variety of scientific fields and has previously been used to determine the global solar wind relationship with the radiation belts [*Balikhin et al.*, 2011, 2012; *Boynton et al.*, 2013] and with geomagnetic storms [*Boynton et al.*, 2011].

The present study aims to gather statistical data of dropouts in electron flux for energies ranging from 24 keV to 2.7 MeV and also to determine what are the main solar wind or geomagnetic conditions leading to these dropouts. Moreover, similar to *Gao et al.* [2015], this study investigates all dropouts regardless of whether they occurred during a geomagnetic storm or not, but over a much wider energy range. The statistics was based on 20 years of data from geosynchronous Los Alamos National Laboratory (LANL) spacecraft. Using the ERR method, the same database has been employed by *Balikhin et al.* [2011] and *Boynton et al.* [2013] to determine the main factors governing global variations of electron flux at all times (i.e., including flux increases as well as decreases or no change), while correlation analyses were performed earlier at MeV energies [*Reeves et al.*, 2011] and over all energies but with a smaller 5 years data subset *Li et al.* [2005]. Here we have rather focused on the sole flux dropouts to search for their peculiar governing factors, which can be different from the factors controlling flux increases. Dropouts have been automatically identified and selected within the LANL data set for each energy channel. The database is discussed in section 2, as well as the way the dropouts were selected. In section 3, the statistical distributions of the waiting time between dropouts and of the magnitude of the dropouts are provided. Section 4 uses the ERR methodology to explore the relationship between the magnitude of the dropouts and external factors, such as solar wind variables and geomagnetic indices.

2. Instruments, Data, and Methodology

The 20 years of electron flux data used in this study come from the Synchronous Orbit Particle Analyzer (SOPA) and Energetic Sensor for Particles (ESP) instruments on board the Los Alamos National Laboratory (LANL) spacecraft, which are situated at Geostationary Earth Orbit (GEO). There are multiple LANL satellites at GEO each with the SOPA and ESP instruments. A uniform daily average of the electron flux was calculated by combining the flux values for each of the energy channels on each satellite. The data cover a period from 22 September 1989 to 31 December 2009. These data are available online at http://onlinelibrary.wiley.com/doi/10.1029/2010JA015735/suppinfo [*Reeves et al.*, 2011].

This study examines 14 energies, ranging from 24.1 keV to 3.5 MeV. The data for the lower 13 energy channels (24.1 keV to 2.0 MeV) are from the SOPA, while the highest energy considered in this study, centered at 2.65 MeV, comes from the ESP. The original energy channels of the SOPA instrument response were modeled by Monte Carlo simulations, as a function of energy and penetrating backgrounds. This was fit to a relativistic bi-Maxwellian spectrum and then employed to evaluate the fluxes at fixed virtual energy channels [*Cayton and Tuszewski*, 2005]. The lowest and highest of these evaluated energies (24.1 keV and 2.0 MeV) were extrapolations of the bi-Maxwellian fit and thus could be not as accurate as the other virtual channels [*Cayton and Tuszewski*, 2005]. A detailed methodology of the data processing can be found in the auxiliary material published with *Reeves et al.* [2011].

The solar wind data for the same time period came from a variety of spacecraft (Interplanetary Monitoring Platform 8, Geotail, Wind, and Advanced Composition Explorer) and were supplied by the OMNI website (http://omniweb.gsfc.nasa.gov). The geomagnetic indices data employed here were also taken from the OMNI website.

Electron flux dropouts often occur over a timescale smaller than a day, and fluxes can then drop by up to several orders of magnitude. In this study, electron flux dropouts were defined as any decrease in flux larger than a factor of 4 in 1 day or a factor of 9 in 2 days, where at least a factor of 2.5 decrease occurred in each day. The second condition was introduced because the daily averaging of the LANL electron flux data used here can potentially smooth a dropout, so that it will not be detected. For example, if a decrease in flux taking place over exactly 1 day were to start at midday on a given day and finish at midday the next day, there would be a less steep drop over both 1 day and 2 days, compared with the same dropout starting just after midnight and ending at midnight of the same day.

Let us emphasize that the required minimum magnitude of the flux decrease (by at least a factor 4) was also chosen so as not to select as a dropout a usual (slow) flux decay due to scattering by chorus waves. *Boynton et al.* [2014] found from an analysis of the same LANL satellite data that electron fluxes at $L = 6.6$ decay exponentially with lifetimes τ_L increasing with energy from $\tau_L = 1-3$ days at 24 keV up to $\tau_L \sim 3-15$ days for MeV electrons, in rough agreement at low energy with lifetime models from *Mourenas et al.* [2012] based on average quiet time levels of chorus wave intensity. Thus, our selection criteria for dropouts ensure that such slower decays will not be considered here as dropouts.

3. Statistical Analysis

Dropouts of the electron flux at GEO were automatically identified for each of the 14 considered energies and then a statistical analysis was performed to derive their principal features. Table 1 shows the number of dropouts identified for each energy. It shows that there were markedly fewer electron flux dropouts in the medium-energy range, between 63 keV and 408 keV than at $E < 63$ keV or $E > 408$ keV.

3.1. Mean Waiting Time Between Consecutive Dropouts

Next, the mean waiting time between two consecutive dropouts was calculated in each energy range. Since there are data gaps within the LANL electron flux data, the waiting time between two successive dropouts was only included in the calculation of the mean value when there was no data gap between these consecutive dropouts. The 10th, 20th, 30th, 40th, 50th, 60th, 70th, 80th, and 90th percentiles of the distribution were also found the same way. They are provided in Table 2 and also displayed in Figure 1. It is worth noting the large mean waiting time $T_w \sim 40-100$ days between dropouts at medium energies from 63 keV to 408 keV, while it is significantly smaller at lower or higher energies ($E < 63$ keV or $E > 408$ keV), where $T_w \sim 10-25$ days. The larger spread of the distribution in the medium-energy range probably stems partly from the fact that fewer dropouts were observed in this range.

3.2. Magnitude of the Dropouts

The dropout magnitude was defined as the factor by which the electron flux has decreased. Therefore, it was calculated by dividing the electron flux at the start of each dropout by the flux at the end of the dropout (some dropouts take place over 2 days). The mean and the 10th, 20th, 30th, 40th, 50th, 60th, 70th, 80th, and 90th percentiles of the distribution are shown in Table 3 and Figure 2.

For 1.3 MeV and 2 MeV electron fluxes, the mean dropout magnitude happens to be greater than the 90th percentile. This is due to a small number of extremely large dropouts, similar to the one displayed in Figure 3. The mean and 90th percentile dropout magnitudes are noticeably constant from 24 keV to 650 keV with values

Table 1. Table Showing the Number of Dropouts Identified for Each of the Energies Studied

Energy	No. of Dropouts
24 keV	235
31 keV	186
42 keV	129
63 keV	58
90 keV	29
128 keV	25
173 keV	37
270 keV	44
408 keV	78
625 keV	178
925 keV	429
1.3 MeV	655
2 MeV	901
2.7 MeV	476

of 7–8 and 8–10, respectively. At higher energy $E \geq 1.3$ MeV, both the mean and 80th percentile dropout magnitudes increase significantly above 11–12, reaching factors of ~20–100 at ~1.3–2 MeV.

3.3. Discussion of the Results

Some of the observed dropouts may partially correspond to electron PSD redistribution within the outer belt. This occurs mainly in the case of outward radial transport, when electrons in a given energy range at GEO are replaced by much less numerous particles of initially higher energy coming from lower L shells and decelerated (by conservation of their first adiabatic invariant) as they move outward to GEO, in association with a decrease of the magnetic field strength (the outward motion of electrons resulting from conservation of their third adiabatic invariant) [*Kim and Chan*, 1997; *Turner et al.*, 2012b, 2013]. However, the very different dropout occurrences in the low-energy (20–65 keV) and medium-energy (65–600 keV) ranges (see Figure 1), together with the very similar dropout magnitudes in the same energy ranges, suggest that this reversible mechanism is probably not prevalent. First, if the reduction of dropout occurrences at medium energy were caused by a corresponding reduction of dropout magnitude due to radial transport combined with different slopes of the PSD roughly power law energy distribution PSD(E) $\sim E^{-A}$ in the low- and medium-energy ranges, then

Table 2. Table Showing the Mean Time Between Dropouts for Each of the 14 Energies Along With the 10th, 20th, 30th, 40th, 50th, 60th, 70th, 80th, and 90th Percentiles of the Distribution

Energy	Mean (days)	10%	20%	30%	40%	50%	60%	70%	80%	90%
24 keV	18.92	3	4	5.9	9	11	14	20	28	45
31 keV	22.5	3	4	6.7	9	13	17.9	22.3	35.4	53
42 keV	27.85	3	5	7	10	14	21.9	33.4	46	65.6
63 keV	40.04	4.2	11	13.8	19.1	25	45.3	52.1	56.8	102.9
90 keV	72.5	12	20	42.5	64	70.5	74	97	117.5	140.5
128 keV	98.75	11.6	17.5	53.5	69.2	95.5	117.3	122.5	158.5	214.1
173 keV	70	10.7	12.8	29.4	54.9	69	74	100.1	118.6	142
270 keV	55	10	11.5	13	18.5	35	41	51	106	163
408 keV	42.79	5.8	14	15.4	19.9	36.5	40.8	52.6	71.7	91.1
625 keV	25.39	6	9	11	13	16	19.7	29.4	42.1	54.8
925 keV	14.99	4	6	8	9.5	11	13	17	22	31
1.3 MeV	10.22	3	5	7	8	9	10	12	14	18
2 MeV	7.501	3	4	5	6	7	8	9	10	13
2.7 MeV	13.47	4	6	8	9	11	12	15	19	26

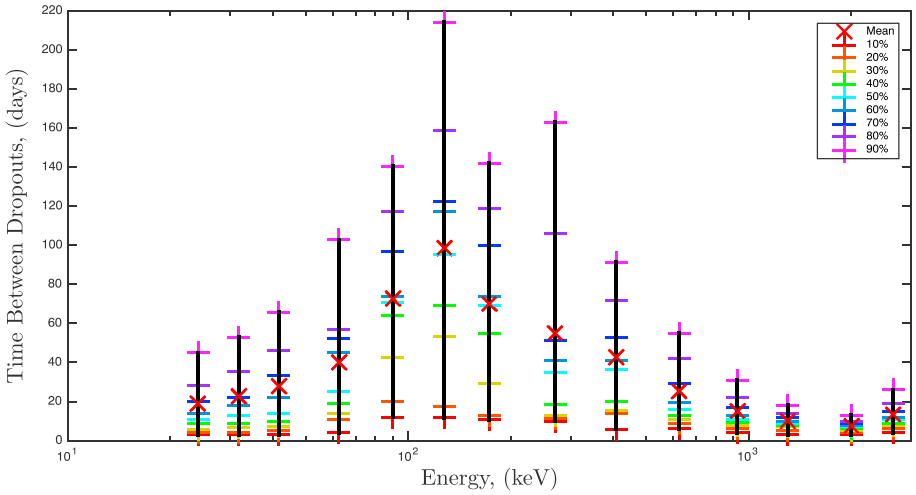

Figure 1. The mean time between dropouts for each of the 14 energies (black cross) along with the 10th (red), 20th (orange), 30th (yellow), 40th (green), 50th (cyan), 60th (light blue), 70th (dark blue), 80th (purple), and 90th (magenta) percentiles of the distribution.

the mean magnitude of dropouts would be expected to be reduced in the medium-energy range (at least for a random, Gaussian-like distribution), contrary to the results in Figure 2. Actually, the energy distribution of the electron PSD at $L \sim 5-6.6$ usually follows a roughly constant power law form, as energy increases between 25 keV and 500 keV, with a constant or slightly increasing exponent A [e.g., see *Sicard-Piet et al.*, 2008; *Johnston et al.*, 2014]: in this case, radial transport alone should lead to roughly similar dropout magnitudes and occurrences in both energy ranges, contrary to the statistical results in Figures 1 and 2. In addition, the sudden increase of dropout magnitude as energy increases between 0.9 MeV and 1.3 MeV in Figure 2 cannot be explained by the sole effect of outward radial transport: this would require a significant increase of the exponent A of the power law energy distribution of the PSD occurring regularly just above 1 MeV (at $\simeq$1.3–2 MeV) at $L \sim 5-6.6$, while observations generally do not show such a strong inflection there, except during periods of energization and related enhancements of the PSD [e.g., see *Sicard-Piet et al.*, 2008; *Johnston et al.*, 2014; *Li et al.*, 2014]. Taken together, the above considerations suggest that the reversible mechanism of radial redistribution of electrons is not the main governing factor in these dropouts, consistent with previous studies [*Turner et al.*, 2013].

Table 3. Table Showing the Mean Magnitude of the Dropouts for Each of the 14 Energies Along With the 10th, 20th, 30th, 40th, 50th, 60th, 70th, 80th, and 90th Percentiles of the Distribution

Energy	Mean	10%	20%	30%	40%	50%	60%	70%	80%	90%
24 keV	7.195	4.157	4.375	4.628	4.927	5.197	5.633	6.727	7.988	9.996
31 keV	6.958	4.103	4.321	4.482	4.682	5.068	5.76	6.519	7.907	10.1
42 keV	6.819	4.111	4.254	4.416	4.673	5.159	5.798	6.627	7.64	9.143
63 keV	6.969	4.176	4.344	4.61	4.779	5.04	5.47	5.808	7.408	9.448
90 keV	7.792	4.139	4.223	4.454	4.695	5.501	6.352	7.903	8.872	11.64
128 keV	7.669	4.213	4.455	4.713	4.952	5.348	6.636	7.39	10.27	11.62
173 keV	6.891	4.112	4.384	4.735	5.206	5.367	6.369	7.643	8.202	12.22
270 keV	8.062	4.333	4.688	4.956	5.565	6.17	7.029	8.327	9.843	12.46
408 keV	7.067	4.059	4.184	4.426	4.6	4.937	5.422	6.305	7.374	10.87
625 keV	8.738	4.173	4.473	4.787	5.157	5.611	6.424	7.722	9.154	11.98
925 keV	14.13	4.037	4.357	4.857	5.41	6.251	7.379	8.585	10.8	17.1
1.3 MeV	47.78	4.236	4.784	5.4	6.213	7.628	9.876	12.74	16.81	33.18
2 MeV	287.7	4.548	5.598	6.582	8.425	11.15	15.32	23.7	40.4	124.7
2.7 MeV	11.09	4.145	4.524	5.041	5.667	6.394	7.477	8.985	11.82	16.94

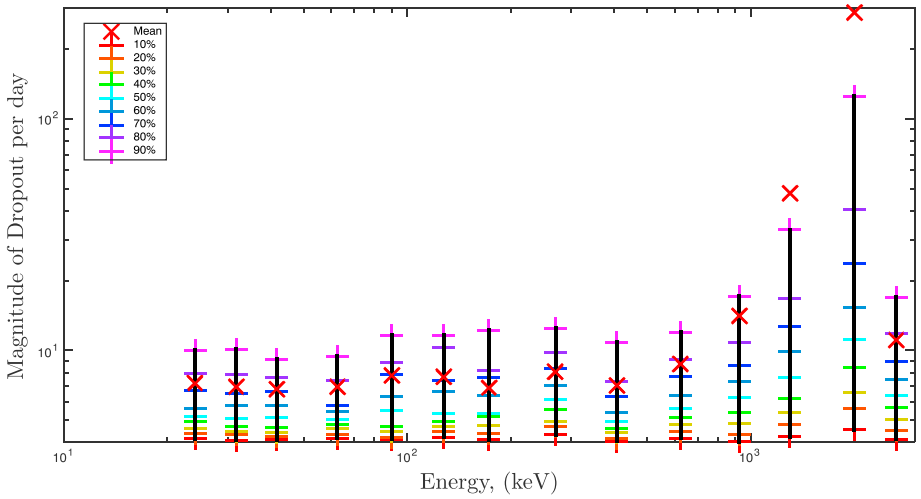

Figure 2. The magnitude of dropouts for each of the 14 energies (black cross) along with the 10th (red), 20th (orange), 30th (yellow), 40th (green), 50th (cyan), 60th (light blue), 70th (dark blue), 80th (purple), and 90th (magenta) percentiles of the distribution.

For similar reasons, magnetopause shadowing (in the presence of a compressed magnetosphere) coupled with enhanced outward radial diffusion by ULF waves [*Turner et al.*, 2012b] may not be the sole (nor sometimes the main) driver of dropouts either. The dominant electrostatic radial diffusion rates are independent of electron energy in this region and should lead to roughly similar effects at all energies [*Ozeke et al.*, 2014]. This is again in clear contradiction with the very different dropout occurrences and magnitudes in the low-energy (<65 keV), medium-energy (65–600 keV), and high-energy (600–2650 keV) ranges, implying that different phenomena are probably governing dropout occurrences and magnitudes in these different energy domains. Nevertheless, various studies have also demonstrated that there are often positive (negative) radial gradients in low-energy (high-energy) electron PSD, with a transition occurring for a magnetic moment of about 200 MeV/G, corresponding at $L = 6.6$ to $E \sim 0.2$ MeV [e.g., see *Turner et al.*, 2012a]. Since radial diffusion preferentially scatters particles toward lower PSD, it may amplify any decrease of flux at high-energy $E \geq 0.2$ MeV (and consequently also the occurrences of strong dropouts) by rapidly scattering high-energy electrons toward the magnetopause. Conversely, at lower energy $E < 0.2$ MeV, radial diffusion can certainly mitigate the magnitude (and occurrences) of dropouts by replacing low-energy electrons by more numerous lower energy particles arriving (and accelerated) from higher L [*Turner et al.*, 2013]. Therefore, radial diffusion and magnetopause shadowing likely play an important role in a significant portion of the considered dropouts

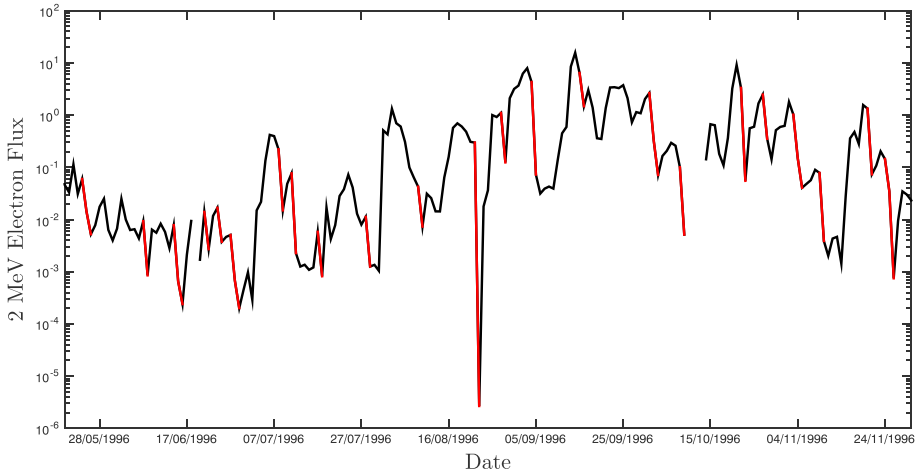

Figure 3. An extremely large dropout on 23 August 1996 in the 2 MeV electron flux where the magnitude of the dropout is $>10^5$. The dropouts are shown in red.

[*Turner et al.*, 2012b, 2013]. Notwithstanding, there is no apparent threshold in Figures 1 and 2 separating low dropout magnitudes and occurrences below 0.2 MeV from high dropout magnitudes and occurrences above it. It is an indication that other dropout mechanisms are probably operating in some energy ranges.

But which other mechanisms? In which energy ranges? Losses due to field line stretching near midnight during strong disturbances [*Artemyev et al.*, 2013], as well as precipitation due to intense EMIC waves, occur preferentially at high (MeV) energies [*Summers and Thorne*, 2003; *Blum et al.*, 2015; *Yu et al.*, 2015] and could contribute to the higher magnitudes and occurrences of dropouts at such high energies as compared with the range $E \sim 0.1-0.5$ MeV. However, strong dropouts (i.e., extending up to equatorial pitch angles ~90°) at relatively moderate energies ~1.3–2.65 MeV induced by EMIC waves would require intense and widespread waves at frequencies very close to the helium ion gyrofrequency [*Ukhorskiy et al.*, 2010], which does not seem to be a very usual situation [*Kersten et al.*, 2014] due to strong damping [*Chen et al.*, 2013]. As an alternative and possibly more realistic scenario, it has been suggested that some fast and strong dropouts could be produced by the combined effects of typical EMIC and lower band chorus waves present in the same or different MLT sectors [*Mourenas et al.*, 2016b].

In contrast with EMIC waves, chorus waves are present only in the low plasma density region outside the plasmasphere. Thus, the plasmapause needs to be located at $L = L_{pp} < 6.5$ for chorus waves to potentially affect electron fluxes at GEO. Based on the plasmapause model from *O'Brien and Moldwin* [2003], it requires $Kp \geq 1$ or $AE > 120$ nT. Moreover, chorus (and EMIC) waves become more intense as *AE* or *Kp* increase, or *Dst* decreases [e.g., see *Agapitov et al.*, 2015]. Consequently, chorus (and EMIC) waves should become effective in electron dropouts at GEO mainly during disturbed geomagnetic conditions such that $AE \geq 400$ nT, $Kp \geq 4$, or $Dst < -30$ nT [*Mourenas et al.*, 2016b; *Agapitov et al.*, 2015].

It is worth noting that 40% of the 270 keV dropouts and 55% of the 1.3 MeV dropouts have magnitudes larger than 7, well above the threshold used in the present study: Thus, the bulk of the distributions of dropout magnitudes are not very different in these different energy ranges. However, the tail of the distribution of dropout magnitudes is very different, with 20% of the dropouts having a magnitude larger than 17 at 1.3 MeV, while 20% of the dropouts have a magnitude larger than 10 at 270 keV. Thus, it is the tail of the distribution that accounts for most of the significant increase in mean and median dropout magnitudes in the high (MeV) energy range. It indicates that some of the MeV electron dropouts are likely partially governed by some mechanisms different from the mechanisms prevalent at lower energy. The much steeper electron flux decrease observed during some MeV dropouts may be produced by field line curvature effects near midnight during strong magnetic disturbances [*Artemyev et al.*, 2013], or they may correspond to strong precipitation induced by combined EMIC and chorus waves [*Summers and Thorne*, 2003; *Blum et al.*, 2015; *Gao et al.*, 2015; *Yu et al.*, 2015; *Mourenas et al.*, 2016b]—two loss processes which are both strongly energy dependent.

At low energy, loss timescales due to quasi-linear pitch angle scattering by typical whistler mode chorus waves vary with energy like $E^{3/2}$ [*Mourenas et al.*, 2012] and can reach very small values of 1–2 days at $E < 65$ keV, even during moderately disturbed periods [*Boynton et al.*, 2014]. Thus, when azimuthal drift-averaged quasi-parallel chorus wave amplitudes are enhanced during substorms to values >20(50) pT, they can lead to faster flux decays at $E < 100(250)$ keV [*Mourenas et al.*, 2012], which will be counted as dropouts in the present study. The presence of bursts of oblique and parallel intense chorus waves could also lead to very fast dropouts via nonlinear effects (trapping and phase bunching) at $E < 100-150$ keV [*Mourenas et al.*, 2016a].

Various combinations of the different aforementioned phenomena might explain the larger occurrences of dropouts at lower and higher energies as compared with the medium-range $E \sim 0.1-0.5$ MeV, and the corresponding smaller waiting times between consecutive dropouts. The relatively low waiting time between dropouts at relativistic energies may have important consequences on the risks posed by elevated MeV electron fluxes to geostationary satellites (possibly also to GPS satellites if the dropouts extend to $L \sim 4.5$). These low waiting times mean that on average, any very strong increase of ~1–3 MeV electron flux (due to any particular disturbance) should be wiped out after about 5 days—limiting the time-integrated radiation dose (at least for a while, before the next flux increase). The same should be true for spacecraft surface charging due to high fluxes of less than 50 keV electrons.

4. Solar Wind and Geomagnetic Activity Influence on Dropouts

4.1. State of the Art

In a seminal paper, *Dungey* [1961] suggested that the dynamics of the magnetosphere was controlled by both the solar wind and the interplanetary magnetic field (IMF). The main factor that is thought to produce dropouts is solar wind dynamic pressure. An increase in dynamic pressure compresses the magnetosphere, causing trapped electrons in the outer radiation belt to be lost to the solar wind via magnetopause shadowing. After this initial loss, outward radial diffusion depletes electron fluxes closer to the Earth, causing a dropout across a wide range of L shells often reaching $L \sim 4.5-5$. *Green et al.* [2004] demonstrated statistically that dropouts often occur with the onset of a southward IMF and an increase in solar wind density after 1–2 days of calm. It was suggested that the buildup of a cold and dense plasma sheet could later increase the efficiency of loss mechanisms, leading to flux dropouts [*Green et al.*, 2004; *Onsager et al.*, 2007].

Storms are not necessary for dropouts to occur, but dropouts often occur during substorm activity (high *AE*). Using superposed epoch analysis, *Yuan and Zong* [2013] and *Gao et al.* [2015] recently showed evidence that the north-south component of the IMF is indeed an important contributor. An increase of southward IMF can increase the reconnection rate on the dayside, enhancing transport toward the magnetotail and ultimately leading to the penetration of anisotropic plasma sheet electron and proton populations into the inner magnetosphere. These unstable particle populations may in turn excite various waves (EMIC, chorus, and magnetosonic) which may scatter electrons toward their loss cone, leading to their precipitation.

Solar wind density is also expected to play a role. *Borovsky and Denton* [2009] found that many relativistic electron dropouts occurring during storm onsets are temporally associated with (i) an enhanced solar wind density, (ii) enhanced magnetospheric convection (*Kp*), (iii) the appearance of a denser plasma sheet following the solar wind density enhancement after a delay of a few hours [*Denton and Borovsky*, 2009], (iv) the formation of a plasmaspheric plume, and (v) a sensible increase of $|Dst|$ (or equivalently *SYM-H*). Enhancements of plasma sheet density induced by increased solar wind density may reduce the penetration of large-scale electric fields into the inner magnetosphere, increasing the size of the plasmasphere and of high-density regions (like plumes) around it, potentially allowing stronger EMIC wave growth near $L = 6.6$ and subsequent relativistic electron scattering into the atmosphere [*Onsager et al.*, 2007; *Lyatsky and Khazanov*, 2008].

Lopez et al. [2004] showed on the basis of MHD simulations that during periods of strong southward IMF, an increase of the solar wind density may increase the reconnection rate [see also *Lavraud and Borovsky*, 2008]. *Lyatsky and Khazanov* [2008] further hinted that solar wind density might be a more important controlling factor of relativistic electron fluxes at geostationary orbit than solar wind velocity over shorter timescales (less than 10 h) following the start of solar wind changes (similar results were obtained by *Potapov et al.* [2014], in their Figure 3), with a larger density corresponding to lower electron fluxes. *Balikhin et al.* [2011] and *Boynton et al.* [2013] found that the solar wind density controls a majority of the 1.8–3.5 MeV electron flux variance, and a similar anticorrelation was also found by *Hartley et al.* [2014]. Thus, increases of southward IMF B_s or solar wind dynamic pressure p, as well as increases of the solar wind density n, may all concur to various degrees, together or separately, to produce strong electron flux dropouts in various energy ranges.

4.2. ERR Analysis

In this study, the Error Reduction Ratio (ERR) analysis [*Billings et al.*, 1988; *Boynton et al.*, 2011] has been used to find the main relationships existing between dropouts at geosynchronous orbit and external factors, such as solar wind parameters and geomagnetic conditions. This method is able to automatically deduce the most influential parameters, or combinations of parameters, from input-output data. This methodology is similar to a correlation analysis, but it is able to reveal a wide class of nonlinearities, while the correlation analysis is unsuitable for nonlinear systems [*Billings et al.*, 1988; *Balikhin et al.*, 2011; *Boynton et al.*, 2011]. For this study, the structure can be represented mathematically as follows:

$$y(t) = F[u_1(t-1), \ldots, u_1(t-n_{u_1}), \ldots, \quad u_m(t-1), \ldots, u_m(t-n_{u_m}), \ldots. \tag{1}$$

In equation (1), it is assumed that the output y at a time t can be represented by a polynomial function F, made up of m lagged input terms, $u_1, \ldots, u_m$, combined to a nonlinear degree, where the maximum lag for each input is represented by n_{u_i}. The ERR algorithm then identifies the most significant term, searching through all the possible linear and nonlinear combinations, by use of the ERR. After the first term is found, its influence is removed by an orthogonalization of all the remaining terms with respect to the previously found term and the ERR is used again to find the most significant orthogonalized term. This process is repeated until all

Table 4. ERR Analysis Results of the Dropout Factor, Where the Input Vales Were the Daily Maximum Solar Wind Velocity, Density and Dynamic Pressure; Daily Maximum IMF Magnitude and the Southward IMF; and the Daily Maximum *AE* Index and the Daily Minimum *SYM-H* Index

Energy	First Term	Second Term	Third Term
24 keV	$AE(t-1)$	$AE(t-0)V(t-1)$	$p(t-2)$
31 keV	$AE(t-1)$	$AE(t-0)V(t-1)$	$p(t-2)$
42 keV	$AE(t-1)$	$AE(t-0)V(t-1)$	$AE(t-2)n(t-1)$
63 keV	$AE(t-2)n(t-1)$	$p(t-1)B(t-2)$	$AE(t-1)^2$
90 keV	$AE(t-2)n(t-1)$	$p(t-1)n(t-0)$	$B_s(t-0)n(t-1)$
128 keV	$p(t-1)n(t-0)$	$AE(t-0)n(t-0)$	$p(t-0)AE(t-1)$
173 keV	$p(t-1)n(t-0)$	$AE(t-0)n(t-1)$	$n(t-0)^2$
270 keV	$p(t-1)n(t-0)$	$AE(t-0)n(t-1)$	$p(t-2)B_s(t-1)$
408 keV	$p(t-1)n(t-0)$	$AE(t-0)n(t-1)$	$p(t-0)SYM\text{-}H(t-0)$
625 keV	$p(t-1)n(t-0)$	$B_s(t-0)n(t-1)$	$B(t-0)n(t-1)$
925 keV	$p(t-1)n(t-0)$	$B_s(t-0)n(t-1)$	$B(t-0)n(t-1)$
1.3 MeV	$p(t-0)B_s(t-1)$	$p(t-0)B(t-2)$	$p(t-1)B_s(t-0)$
2 MeV	$p(t-1)B_s(t-1)$	$p(t-1)AE(t-0)$	$p(t-1)B(t-0)$
2.7 MeV	$p(t-1)n(t-0)$	$SYM\text{-}H(t-0)^2$	$SYM\text{-}H(t-0)n(t-1)$

the significant terms have been found. The advantage of the ERR analysis over the correlation function is its inherent ability to identify nonlinear control parameters and also to separate out the influences of different factors.

4.3. ERR Analysis of the Dropouts

The output data employed in the present analysis were the magnitude of the dropouts detected over 20 years of measurements, defined as the after to before dropout electron flux ratio. Data values were set to zero when no dropouts were observed. The input values were chosen as the daily maximum solar wind velocity V, density n, and dynamic pressure p; daily maximum magnitude B of the interplanetary magnetic field (IMF) and B_s of the southward IMF; and the daily maximum *AE* index and the daily minimum *SYM-H* index. The algorithm was set to search for lagged influences up to 2 days in the past and terms with up to a second degree of nonlinearity.

The results of the ERR analysis are provided in Table 4, which shows the first, second, and third most important governing terms according to their ERR ranking. The *AE* index is the main controlling factor for dropouts occurring at low electron energies (24-42 keV). Next, *AE* is coupled with solar wind density n for 63 keV and 90 keV energies as the term with the highest ERR. At higher energies ($E \geq 128$ keV), the solar wind dynamic pressure p has always a large influence on the magnitude of the dropouts. In the medium-energy range from 128 keV to 925 keV, the term with the highest ERR is the solar wind dynamic pressure p coupled with solar wind density n, although *AE* still appears in the second term over the range 128–408 keV.

At still higher energies $E \sim 1.3$–2 MeV, the main governing term becomes the solar wind dynamic pressure p coupled with southward IMF B_s instead of solar wind density n. At 2.7 MeV, however, solar wind dynamic pressure p coupled with solar wind density n prevails again, although it is worth noting that the squared *SYM-H* turns out to be the second most important term, further appearing also in the third most important term. Time lags are usually found in the range 0–1 day, showing the fast reaction of the electron flux to the conditions leading to dropouts. The fact that the main driving factor at 2.7 MeV is the same as in the medium-energy range (~0.12–0.6 MeV), and different from the main identified driver at 1.3–2 MeV, could be an indication that all the driving factors p, n, and IMF B_s (or *SYM-H*) are important for dropouts at high energy, with no clear prevalence of one factor over the others. But it could also stem from the very different origins of the respective data: electron flux data at 2.7 MeV come from a different instrument (ESP) than the 1.3–2 MeV data (SOPA) and were not postprocessed contrary to lower energy data [*Reeves et al.*, 2011]. During strong dropouts, the measured electron fluxes at 2.7 MeV might sometimes get close to the noise level of the instrument, reducing the apparent magnitude of the strongest dropouts. This would be consistent with results shown in Figure 2, where the 40th percentile dropout magnitudes are similar at 2.7 MeV and 1.3–2 MeV, while the 90th percentile dropout magnitude is much smaller at 2.7 MeV. Since it would reduce the apparent magnitude of the strongest dropouts possibly related to EMIC and chorus waves or magnetic field line stretching, it could lead to a bias

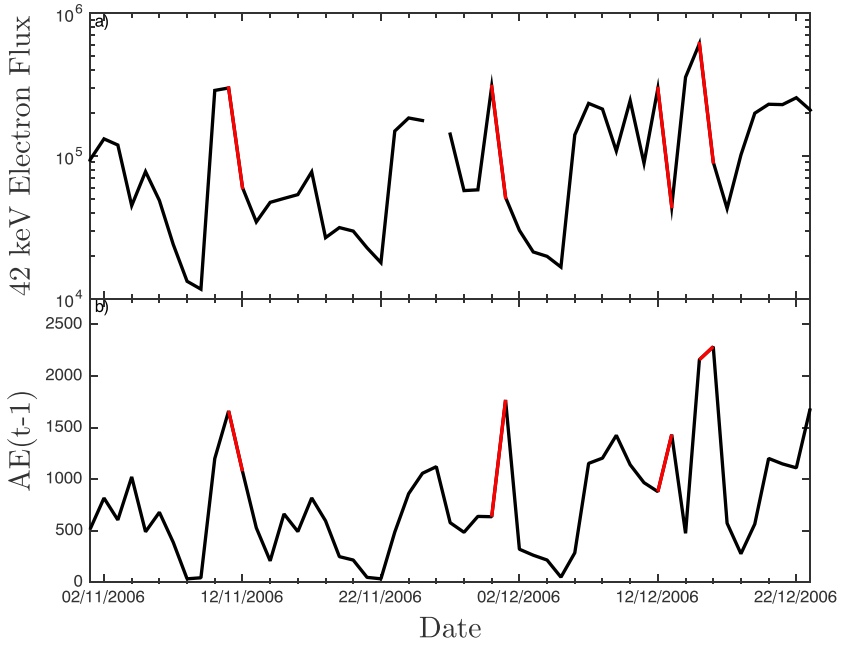

Figure 4. The measured 42 keV electron flux is plotted together with the daily maximum *AE* index from the previous day. The identified dropouts are in red.

toward selecting *p* and *n* rather than an IMF B_s or *SYM-H* as the main drivers of dropouts at 2.7 MeV. A detailed investigation of the differences between data at 2.7 MeV and 1.3 – 2 MeV would be interesting, but it is beyond the scope of the present paper.

The results show that the lower energy dropouts are influenced by the *AE* index. For energies below 500 keV, the *AE* index always appears in the first or second most important terms. Figure 4 shows the measured 42 keV electron flux, where dropouts are shown in red, along with the term with the highest ERR, the daily maximum

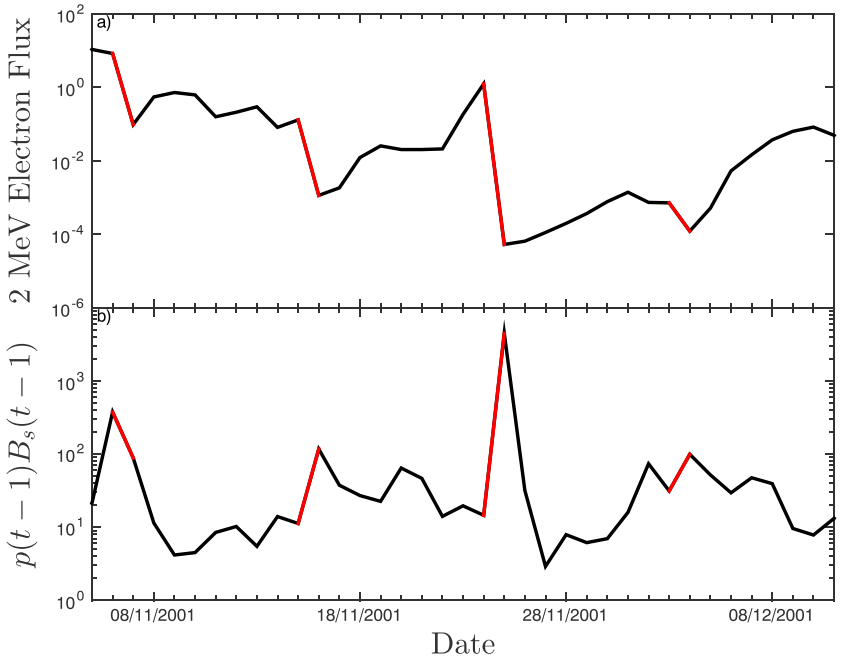

Figure 5. The measured 2 MeV electron flux is plotted together with the daily maximum pressure coupled with the daily maximum southward IMF from the previous day. The identified dropouts are in red.

AE index for the previous day. These dropouts occur preferentially when the *AE* index has been high on the preceding day, in agreement with past studies [*Lam et al.*, 2010]. For energies ≥128 keV, terms that include the solar wind dynamic pressure have the highest ERR. This is also in accordance with various studies on electron flux dropouts [e.g., see *Turner et al.*, 2012b; *Gao et al.*, 2015]. The pressure is coupled with the density for most energies, apart from the two energy channels that observed extreme dropouts, where dropout factors were up to 10^5. Figure 5 shows measured electron flux variations during such an extreme dropout on the 25 November 2001. Here the coupled pressure and southward IMF combine to give an extremely large value relative to the rest of the increases. Nevertheless, note that even the median value of dropout magnitude remains higher at high energy than at energies lower than 1 MeV.

The above results suggest that radial diffusion coupled with magnetopause shadowing may not be the sole, nor maybe the main, driving factor for dropouts. At energies above 1 MeV, strong precipitation induced by EMIC and chorus (or hiss) waves may also be effective [*Blum et al.*, 2015; *Gao et al.*, 2015; *Yu et al.*, 2015; *Mourenas et al.*, 2016b], as well as scattering due to increased field line curvature [*Artemyev et al.*, 2013]—two processes that should usually take place during periods of increased southward IMF or *SYM-H* and that act preferentially at energies $E > 1-2$ MeV. At low energy $E \leq 300$ keV, the observed dropouts can be partially due to chorus wave scattering [*Lam et al.*, 2010; *Mourenas et al.*, 2012]. Chorus wave occurrences and intensities are known to be well described by the *AE* and *Kp* indexes [e.g., see *Agapitov et al.*, 2015] and the level of 30–100 keV electron precipitation has been shown to correlate well with *AE* [*Lam et al.*, 2010]. However, the magnitude of dropouts due to chorus is expected to increase as energy decreases [*Mourenas et al.*, 2012], while it remains quite constant here. One possible explanation is that the increase of losses due to chorus scattering in the lower energy range $E \leq 60$ keV could be mitigated by incoming fluxes of electrons arriving from the plasma sheet with typical energies ~1–50 keV. Such electron injections are indeed frequent during high *AE* periods such as substorms. In the intermediate energy range ~100–500 keV, radial diffusion coupled with magnetopause shadowing, related to large solar wind pressure pulses, is probably the dominant cause of dropouts, with only a moderate contribution from chorus wave scattering (consistent with *AE* still appearing in the second most important governing factor).

5. Geosynchronous Phase Space Density Dropouts at Fixed First Adiabatic Invariant

The so-called *Dst* effect is caused by geomagnetic storms increasing in the ring current, leading to a decrease in the strength of the magnetic field. This, in turn, results in a deceleration of electrons (to conserve their first adiabatic invariant) and their outward motion (to conserve the third adiabatic invariant), possibly leading to local dropouts. Once the storm has died down and the ring current recovers, however, the magnetic field increases again, reaccelerating the electrons and moving them back toward the Earth, increasing back the local electron PSD to initial (or similar) levels. The corresponding dropouts being merely reversible adiabatic processes, it would be nice to be able to directly evaluate their relative proportion in the observed flux dropouts, in order to determine to what extent dropouts seen at GEO are affected by real loss to the atmosphere or at the magnetopause. But this would require the examination of the radial profile of the electron PSD at fixed first adiabatic invariant μ [e.g., see *Kim and Chan*, 1997; *Turner et al.*, 2013], while measurements from LANL satellites are only available at one fixed radial location (at GEO). Thus, we cannot provide an exact evaluation of this reversible *Dst* effect from the sole LANL spacecraft data. Nevertheless, we can still provide good upper bound estimates of this effect in the high-energy range ~0.5–2.7 MeV (see detailed explanations below), building on the fact that the corresponding radial profiles of the electron PSD are generally either roughly constant or decreasing toward higher L over the region $L \sim 5-6.6$ [*Kim and Chan*, 1997; *Turner et al.*, 2012b].

Accordingly, reversible adiabatic dropouts have been sought with the use of the GOES magnetic field data. Magnetic field data at GEO were taken from the magnetometer on board GOES satellites. During the 20 year time period employed for this study, many different GOES satellites were in use. GOES 6 and 7 were both in use from 1989 to 1995 when GOES 8 replaced GOES 6 and a year later in 1996, when GOES 7 was replaced by GOES 9. These were later replaced by GOES 10, 11, 12, and 13. Therefore, magnetic field data were used from all these satellites to create daily average GEO magnetic field data for the 20 year period (dropouts occurring when magnetic field data was missing were excluded). Assuming a roughly constant radial PSD profile at $L \sim 5-6.6$, the ratio R of the electron PSD (at fixed first adiabatic invariant) at a time t_2 (corresponding to dropout) over its

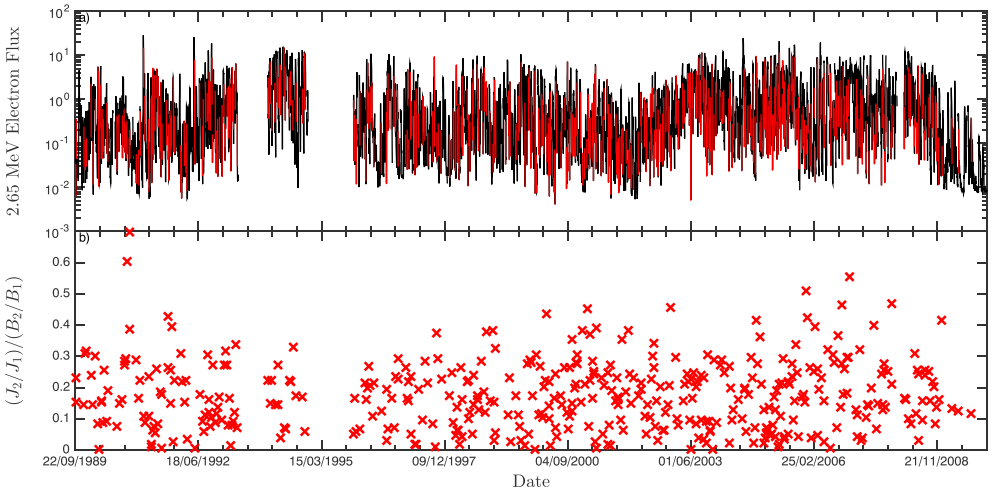

Figure 6. (a) The 2.65 MeV electron flux for the period from 22 September 1989 to 31 December 2009, where the red parts indicate dropouts. (b) The ratio $(J(E_2, t_2)/J(E_1, t_1))/(B(t_2)/B(t_1))$.

level at a time t_1 (immediately before dropout) can be estimated as $R = (J(E_2, t_2)/J(E_1, t_1))/(B(t_2)/B(t_1))$, with J the electron flux, B the GEO magnetic field, E_2 a given energy channel considered at time t_2, and E_1 is calculated at t_1 from the conservation of the first adiabatic invariant [e.g., see *Kim and Chan*, 1997]. The flux $J(E_1, t_1)$ was estimated from available energy channels through logarithmic interpolation. The above expression for R has been derived under the assumption that the radial PSD profile is roughly constant. It allows us to use $J(E_1, t_1)$ evaluated at $L = L_2 = 6.6$. But if the PSD actually decreases toward higher L, $J(E_1, t_1, L_2)$ should be replaced in the expression of R by a higher value $J(E_1, t_1, L_1)$ evaluated at $L_1 < L_2$, which would diminish R. Therefore, the R value obtained when using only fluxes measured at $L = 6.6$ should generally represent a good estimate if the radial PSD profile is roughly constant, or an overestimate if the PSD decreases as L increases—the two most common situations in the range ~0.5–2.7 MeV at $L \sim 5$–6.6 [*Kim and Chan*, 1997; *Turner et al.*, 2012b].

Figure 6a shows the 2.65 MeV electron flux for the entire 20 year period. The red parts indicate the identified dropouts, while Figure 6b shows the corresponding ratio R. One can see that less than 9% of all the dropouts have $R > 0.3$ and less than 3% have $R > 0.4$, most of them having rather $R < 1/4$. Thus, most of the considered flux dropouts are likely to be also real PSD dropouts. The same analysis was repeated for all relativistic energies down to $E = 0.4$ MeV, with similar results.

6. Conclusions

Statistics of electron flux dropouts at geostationary orbit have been provided and analyzed over a very wide range of energies ~0.024–2.7 MeV. The mean waiting time between dropouts and the mean dropout magnitude, along with their statistical distributions, have been calculated for each energy range. Such results are important for space weather studies, because they may contribute to define the level of integrated radiation dose on satellites. It turns out that there are much less numerous dropouts in the medium-energy range, between 63 keV and 450–650 keV than at $E < 63$ keV or $E > 450$–650 keV. Moreover, the magnitude of the dropouts remains nearly constant as electron energy increases up to 1 MeV, increasing strongly above 1 MeV. It suggests that different phenomena prevail in these different energy ranges.

Another aim of the present study was to identify the solar wind or geomagnetic conditions that led to dropouts and to try to infer the corresponding probable loss processes. The ERR analysis was used to identify any relationship existing between the dropouts and the solar wind conditions or geomagnetic indices. We found that the main factors governing the dropouts are the *AE* index at energies ≤ 90 keV, solar wind dynamic pressure coupled with solar wind density at energies $128 \leq E \leq 925$ keV and 2.7 MeV (with some additional influence of *AE* at 100–400 keV and of *SYM-H* at 2.7 MeV), and solar wind dynamic pressure coupled with southward IMF for energies $1.3 \leq E \leq 2$ MeV.

Taken as a whole, our statistical results suggest that radial diffusion coupled with magnetopause shadowing should not be the sole (nor maybe the main) driving factor for all these dropouts. At relativistic energies

above 1 MeV, precipitation induced by EMIC and chorus (or hiss) waves is probably also effective [*Blum et al.*, 2015; *Gao et al.*, 2015; *Yu et al.*, 2015; *Mourenas et al.*, 2016b], as well as scattering due to increased field line curvature during disturbances [*Artemyev et al.*, 2013]. At intermediate energies $0.1 < E < 1$ MeV, the observed dropouts are probably mostly due to radial diffusion coupled with magnetopause shadowing, related to sudden increases of solar wind dynamic pressure or density, although chorus scattering should also play some role. Finally, in the lowest energy range $E \sim 20-100$ keV, chorus-driven precipitation may prevail together with outward or inward radial diffusion during high *AE* periods.

Acknowledgments
Electron flux data was supplied by LANL (http://onlinelibrary.wiley.com/doi/10.1029/2010JA015735/suppinfo), while the solar wind and geomagnetic indices data were supplied by OMNIweb (http://omniweb.gsfc.nasa.gov). Part of the research done has received funding from the European Union Horizon 2020 Research and Innovation program under grant agreement 637302 PROGRESS. R.J.B. and M.A.B. would like to acknowledge financial support from STFC and EPSRCEP/H00453X-1.

References

Agapitov, O. V., A. V. Artemyev, D. Mourenas, F. S. Mozer, and V. Krasnoselskikh (2015), *Empirical Model of Lower Band Chorus Wave Distribution in the Outer Radiation Belt*, vol. 120, 10,425–10,442.

Artemyev, A. V., K. G. Orlova, D. Mourenas, O. V. Agapitov, and V. V. Krasnoselskikh (2013), Electron pitch-angle diffusion: Resonant scattering by waves vs. nonadiabatic effects, *Ann. Geophys.*, *31*(9), 1485–1490.

Bailey, D. K. (1968), Some quantitative aspects of electron precipitation in and near the auroral zone, *Rev. Geophys.*, *6*(3), 289–346.

Baker, D. N. (2002), How to cope with space weather, *Science*, *297*(5586), 1486–1487.

Balikhin, M. A., R. J. Boynton, S. N. Walker, J. E. Borovsky, S. A. Billings, and H. L. Wei (2011), Using the NARMAX approach to model the evolution of energetic electrons fluxes at geostationary orbit, *Geophys. Res. Lett.*, *38*, L18105, doi:10.1029/2011GL048980.

Balikhin, M. A., M. Gedalin, G. D. Reeves, R. J. Boynton, and S. A. Billings (2012), Time scaling of the electron flux increase at GEO: The local energy diffusion model vs observations, *J. Geophys. Res.*, *117*, A10208, doi:10.1029/2012JA018114.

Balikhin, M. A., et al. (2015), Observations of discrete harmonics emerging from equatorial noise, *Nat. Commun.*, *6*, 7703, doi:10.1038/ncomms8703.

Billings, S., M. Korenberg, and S. Chen (1988), Identification of non-linear output affine systems using an orthogonal least-squares algorithm, *Int. J. Syst. Sci.*, *19*, 1559–1568.

Blum, L. W., et al. (2015), Observations of coincident EMIC wave activity and duskside energetic electron precipitation on 18–19 January 2013, *Geophys. Res. Lett.*, *42*, 5727–5735, doi:10.1002/2015GL065245.

Borovsky, J. E., and M. H. Denton (2009), Relativistic-electron dropouts and recovery: A superposed epoch study of the magnetosphere and the solar wind, *J. Geophys. Res.*, *114*, A02201, doi:10.1029/2008JA013128.

Borovsky, J. E., and M. H. Denton (2010), Magnetic field at geosynchronous orbit during high-speed stream-driven storms: Connections to the solar wind, the plasma sheet, and the outer electron radiation belt, *J. Geophys. Res.*, *115*, A08217, doi:10.1029/2009JA015116.

Bortnik, J., R. M. Thorne, T. P. O'Brien, J. C. Green, R. J. Strangeway, Y. Y. Shprits, and D. N. Baker (2006), Observation of two distinct, rapid loss mechanisms during the 20 November 2003 radiation belt dropout event, *J. Geophys. Res.*, *111*, A12216, doi:10.1029/2006JA011802.

Boynton, R. J., M. A. Balikhin, S. A. Billings, H. L. Wei, and N. Ganushkina (2011), Using the NARMAX OLS-ERR algorithm to obtain the most influential coupling functions that affect the evolution of the magnetosphere, *J. Geophys. Res.*, *116*, A05218, doi:10.1029/2010JA015505.

Boynton, R. J., M. A. Balikhin, S. A. Billings, G. D. Reeves, N. Ganushkina, M. Gedalin, O. A. Amariutei, J. E. Borovsky, and S. N. Walker (2013), The analysis of electron fluxes at geosynchronous orbit employing a NARMAX approach, *J. Geophys. Res. Space Physics*, *118*, 1500–1513, doi:10.1002/jgra.50192.

Boynton, R. J., M. A. Balikhin, and D. Mourenas (2014), Statistical analysis of electron lifetimes at GEO: Comparisons with chorus-driven losses, *J. Geophys. Res. Space Physics*, *119*, 6356–6366, doi:10.1002/2014JA019920.

Cayton, T. E., and M. Tuszewski (2005), *Improved electron fluxes from the synchronous orbit particle analyzer*, vol. 3, S11B05.

Chen, L., R. M. Thorne, Y. Shprits, and B. Ni (2013), An improved dispersion relation for parallel propagating electromagnetic waves in warm plasmas: Application to electron scattering, *J. Geophys. Res. Space Physics*, *118*, 2185–2195, doi:10.1002/jgra.50260.

Denton, M. H., and J. E. Borovsky (2009), The superdense plasma sheet in the magnetosphere during high-speed-stream-driven storms: Plasma transport timescales, *J. Atmos. Sol. Terr. Phys.*, *71*(10-11), 1045–1058.

Dessler, A. J., and R. Karplus (1961), Some effects of diamagnetic ring currents on Van Allen radiation, *J. Geophys. Res.*, *66*(8), 2289–2295.

Dungey, J. W. (1961), Interplanetary magnetic field and auroral zones, *Phys. Rev. Lett.*, *6*, 47–48.

Gao, X., W. Li, J. Bortnik, R. M. Thorne, Q. Lu, Q. Ma, X. Tao, and S. Wang (2015), The effect of different solar wind parameters upon significant relativistic electron flux dropouts in the magnetosphere, *J. Geophys. Res. Space Physics*, *120*, 4324–4337, doi:10.1002/2015JA021182.

Green, J. C., T. G. Onsager, T. P. O'Brien, and D. N. Baker (2004), Testing loss mechanisms capable of rapidly depleting relativistic electron flux in the Earth's outer radiation belt, *J. Geophys. Res.*, *109*, A12211, doi:10.1029/2004JA010579.

Hartley, D. P., M. H. Denton, and J. V. Rodriguez (2014), Electron number density, temperature, and energy density at geo and links to the solar wind: A simple predictive capability, *J. Geophys. Res. Space Physics*, *119*(6), 4556–4571.

Horne, R. B., S. A. Glauert, N. P. Meredith, D. Boscher, V. Maget, D. Heynderickx, and D. Pitchford (2013), Space weather impacts on satellites and forecasting the Earth's electron radiation belts with spacecast, *Space Weather*, *11*, 169–186, doi:10.1002/swe.20023.

Johnston, W. R., T. P. O'Brien, G. P. Ginet, S. L. Huston, T. B. Guild, and J. A. Fennelly (2014), Ae9/ap9/spm: New models for radiation belt and space plasma specification, *Proc. SPIE*, *9085*, 908508, doi:10.1117/12.2049836.

Kersten, T., R. B. Horne, S. A. Glauert, N. P. Meredith, B. J. Fraser, and R. S. Grew (2014), Electron losses from the radiation belts caused by EMIC waves, *J. Geophys. Res. Space Physics*, *119*, 8820–8837, doi:10.1002/2014JA020366.

Kim, H.-J., and A. A. Chan (1997), Fully adiabatic changes in storm time relativistic electron fluxes, *J. Geophys. Res.*, *102*(A10), 22,107–22,116.

Lam, M. M., R. B. Horne, N. P. Meredith, S. A. Glauert, T. Moffat-Griffin, and J. C. Green (2010), Origin of energetic electron precipitation >30 keV into the atmosphere, *J. Geophys. Res.*, *115*, A00F08, doi:10.1029/2009JA014619.

Lavraud, B., and J. E. Borovsky (2008), Altered solar wind-magnetosphere interaction at low mach numbers: Coronal mass ejections, *J. Geophys. Res.*, *113*, A00B08, doi:10.1029/2008JA013192.

Li, W., et al. (2014), Radiation belt electron acceleration by chorus waves during the 17 March 2013 storm, *J. Geophys. Res. Space Physics*, *119*, 4681–4693, doi:10.1002/2014JA019945.

Li, X., D. N. Baker, M. Temerin, G. Reeves, R. Friedel, and C. Shen (2005), Energetic electrons, 50 keV to 6 MeV, at geosynchronous orbit: Their responses to solar wind variations, *Space Weather*, *3*, S04001, doi:10.1029/2004SW000105.

Lopez, R. E., M. Wiltberger, S. Hernandez, and J. G. Lyon (2004), Solar wind density control of energy transfer to the magnetosphere, *Geophys. Res. Lett.*, *31*, L08804, doi:10.1029/2003GL018780.

Lorentzen, K. R., M. D. Looper, and J. B. Blake (2001), Relativistic electron microbursts during the gem storms, *Geophys. Res. Lett.*, *28*(13), 2573–2576.

Lyatsky, W., and G. V. Khazanov (2008), Effect of solar wind density on relativistic electrons at geosynchronous orbit, *Geophys. Res. Lett.*, *35*, L03109, doi:10.1029/2007GL032524.
Maalouf, M., M. Durante, and N. Foray (2011), Biological effects of space radiation on human cells: History, advances and outcomes, *J. Radiat. Res.*, *52*(2), 126–146, doi:10.1269/jrr.10128.
McIlwain, C. E. (1966), Ring current effects on trapped particles, *J. Geophys. Res.*, *71*(15), 3623–3628.
Meredith, N. P., R. B. Horne, S. A. Glauert, R. M. Thorne, D. Summers, J. M. Albert, and R. R. Anderson (2006), Energetic outer zone electron loss timescales during low geomagnetic activity, *J. Geophys. Res.*, *111*, A05212, doi:10.1029/2005JA011516.
Mourenas, D., A. V. Artemyev, J.-F. Ripoll, O. V. Agapitov, and V. V. Krasnoselskikh (2012), Timescales for electron quasi-linear diffusion by parallel and oblique lower-band chorus waves, *J. Geophys. Res.*, *117*, A06234, doi:10.1029/2012JA017717.
Mourenas, D., A. V. Artemyev, O. V. Agapitov, and V. Krasnoselskikh (2013), Analytical estimates of electron quasi-linear diffusion by fast magnetosonic waves, *J. Geophys. Res. Space Phys.*, *118*, 3096–3112, doi:10.1002/jgra.50349.
Mourenas, D., A. V. Artemyev, O. V. Agapitov, F. S. Mozer, and V. V. Krasnoselskikh (2016a), Equatorial electron loss by double resonance with oblique and parallel intense chorus waves, *J. Geophys. Res. Space Physics*, *121*, 4498–4517, doi:10.1002/2015JA022223.
Mourenas, D., A. V. Artemyev, Q. Ma, O. V. Agapitov, and W. Li (2016b), Fast dropouts of multi-MeV electrons due to combined effects of EMIC and whistler mode waves, *Geophys. Res. Lett.*, *43*, 4155–4163, doi:10.1002/2016GL068921.
O'Brien, T. P., and M. B. Moldwin (2003), Empirical plasmapause models from magnetic indices, *Geophys. Res. Lett.*, *30*(4), 1152, doi:10.1029/2002GL016007.
Onsager, T. G., J. C. Green, G. D. Reeves, and H. J. Singer (2007), Solar wind and magnetospheric conditions leading to the abrupt loss of outer radiation belt electrons, *J. Geophys. Res.*, *112*, A01202, doi:10.1029/2006JA011708.
Ozeke, L. G., I. R. Mann, K. R. Murphy, I. Jonathan Rae, and D. K. Milling (2014), Analytic expressions for ULF wave radiation belt radial diffusion coefficients, *J. Geophys. Res. Space Physics*, *119*, 1587–1605, doi:10.1002/2013JA019204.
Potapov, A., B. Tsegmed, and L. Ryzhakova (2014), Solar cycle variation of "killer" electrons at geosynchronous orbit and electron flux correlation with the solar wind parameters and ULF waves intensity, *Acta Astronaut.*, *93*, 55–63.
Reeves, G. D., S. K. Morley, R. H. W. Friedel, M. G. Henderson, T. E. Cayton, G. Cunningham, J. B. Blake, R. A. Christensen, and D. Thomsen (2011), On the relationship between relativistic electron flux and solar wind velocity: Paulikas and Blake revisited, *J. Geophys. Res.*, *116*, A02213, doi:10.1029/2010JA015735.
Sicard-Piet, A., S. Bourdarie, D. Boscher, R. H. W. Friedel, M. Thomsen, T. Goka, H. Matsumoto, and H. Koshiishi (2008), A new international geostationary electron model: Ige-2006, from 1 keV to 5.2 MeV, *Space Weather*, *6*, S07003, doi:10.1029/2007SW000368.
Summers, D., and R. M. Thorne (2003), Relativistic electron pitch-angle scattering by electromagnetic ion cyclotron waves during geomagnetic storms, *J. Geophys. Res.*, *108*(A4), 1143, doi:10.1029/2002JA009489.
Turner, D. L., V. Angelopoulos, Y. Shprits, A. Kellerman, P. Cruce, and D. Larson (2012a), Radial distributions of equatorial phase space density for outer radiation belt electrons, *Geophys. Res. Lett.*, *39*, L09101, doi:10.1029/2012GL051722.
Turner, D. L., Y. Shprits, M. Hartinger, and V. Angelopoulos (2012b), Explaining sudden losses of outer radiation belt electrons during geomagnetic storms, *Nat. Phys.*, *8*(3), 208–212.
Turner, D. L., S. K. Morley, Y. Miyoshi, B. Ni, and C.-L. Huang (2013), Outer radiation belt flux dropouts: Current understanding and unresolved questions, in *Dynamics of the Earth's Radiation Belts and Inner Magnetosphere*, vol. 199, edited by D. Summers et al., pp. 195–212, AGU, Washington, D. C., doi:10.1029/2012GM001310
Ukhorskiy, A. Y., Y. Y. Shprits, B. J. Anderson, K. Takahashi, and R. M. Thorne (2010), Rapid scattering of radiation belt electrons by storm-time EMIC waves, *Geophys. Res. Lett.*, *37*, L09101, doi:10.1029/2010GL042906.
Ukhorskiy, A. Y., M. I. Sitnov, R. M. Millan, B. T. Kress, J. F. Fennell, S. G. Claudepierre, and R. J. Barnes (2015), Global storm time depletion of the outer electron belt, *J. Geophys. Res. Space Physics*, *120*, 2543–2556, doi:10.1002/2014JA020645.
Yu, J., L. Li, J. B. Cao, Z. G. Yuan, G. D. Reeves, D. N. Baker, J. B. Blake, and H. Spence (2015), Multiple loss processes of relativistic electrons outside the heart of outer radiation belt during a storm sudden commencement, *J. Geophys. Res. Space Physics*, *120*, 10,275–10,288, doi:10.1002/2015JA021460.
Yuan, C., and Q. Zong (2013), Relativistic electron fluxes dropout in the outer radiation belt under different solar wind conditions, *J. Geophys. Res. Space Physics*, *118*, 7545–7556, doi:10.1002/2013JA019066.